Lasers in Manufacturing Conference 2025

Laser percussion drilling of additively manufactured titanium parts with ultrashort laser pulses

Daniel Holder[a,b,1], Nathan Gabriel[a], Christian Hagenlocher[a], Thomas Graf[a]

[a]*Institut für Strahlwerkzeuge (IFSW), University of Stuttgart, Pfaffenwaldring 43, 70569 Stuttgart, Germany*
[b]*ARENA2036 Research Campus, Pfaffenwaldring 19, 70569 Stuttgart, Germany*

Abstract

Additive manufacturing via Laser Powder Bed Fusion (LPBF) enables the production of complex, application-specific titanium components for industries such as aerospace, medical, and chemical processing, but the minimum feature size is limited to several hundred micrometers.
This work demonstrates the use of ultrafast laser percussion drilling (260 fs) to overcome this limitation by fabricating precise shallow dimples and deep microholes in LPBF-generated Ti64 parts. The drilling process is analyzed in three phases: initiation, deep hole progression, and through-hole formation.
Dimples as small as 50 µm with laser-induced periodic surface structures (LIPSS, ~1 µm spatial period) were obtained in the initiation phase, highlighting enhanced microstructuring capabilities. The study shows that peak fluence and pulse number are key to controlling dimple geometry, while pulse energy determines the depth progression and achievable depth of deep microholes. Through-holes of 1.5 mm depth and 110 µm diameter were achieved, corresponding to an aspect ratio of 14. The findings demonstrate the feasibility of using ultrafast laser drilling to introduce micrometer features and high-aspect-ratio geometries, broadening the applications of LPBF components in high-precision fields.

Keywords: Laser drilling; ultrashort laser pulses; microholes; additively manufactured parts; titanium

1. Introduction

Additive manufacturing (AM) techniques, particularly Laser Powder Bed Fusion (LPBF), have become increasingly attractive for the production of high-performance metallic components. LPBF enables the realization of complex geometries and customized designs that are difficult or impossible to achieve through conventional subtractive processes. Applications in aerospace, medical implants, and chemical process engineering have especially benefited from the design freedom and material efficiency offered by AM.

However, LPBF is subject to inherent process limitations due to the nature of layer-by-layer melting and solidification of fine metal powders. These limitations include:

- Surface roughness, often exceeding tens of microns due to partially melted particles,
- Waviness, low circularity, and partial closure of small channels and holes,
- Restricted minimum feature size, especially for narrow holes, which are challenging to form with high precision.

These geometric and morphological constraints restrict the functionality of LPBF parts in applications where fluid dynamics, optical clarity, or tribological behavior are critical. To overcome these issues, post-processing techniques are essential. Among these, ultrafast laser micromachining has emerged as a powerful tool for high-precision material removal with minimal heat-affected zones. Ultrashort pulses enable non-thermal ablation mechanisms, making them well-suited for complex features where precision and surface quality are required.

* Corresponding author. Tel.: +49 711 685 69740.
E-mail address: daniel.holder@ifsw.uni-stuttgart.de.

This study investigates the potential of laser percussion drilling with ultrashort laser pulses as a post-processing method for LPBF-manufactured titanium alloy parts. The focus is on Ti6Al4V (Ti64), a widely used aerospace-grade alloy. The drilling process is analyzed in three sequential phases: Initiation of drilling and ablation threshold determination, deep hole formation and its evolution over pulse count, and through-hole formation and final geometry analysis.

2. Materials and Methods

The experiments were conducted on titanium alloy specimens (Ti6Al4V, commonly abbreviated as Ti64) manufactured via LPBF. The titanium powder used had a particle size distribution ranging from 15 µm to 45 µm. The LPBF process was carried out under an argon atmosphere without additional platform heating, using a laser system with a wavelength of 1075 nm, an average power of 155 W, and a beam diameter of 30 µm. A layer thickness of 20 µm was fabricated by scanning along parallel lines with a scanning speed of 1200 mm/s and with hatching distance of 60 µm. The final sample thickness was 1.5 mm. In selected cases, additional sanding or polishing was applied to the surface prior to laser processing to assess surface effects.

The experimental setup used for depth-monitored laser percussion drilling is shown in Fig. 1. The beam was directed through a galvanometer scanner and an F-Theta lens with a focal length of 160 mm. A dichroic mirror was used to combine the beam path with an OCT-based monitoring system. The sample was mounted on a fixed platform during the laser percussion drilling process.

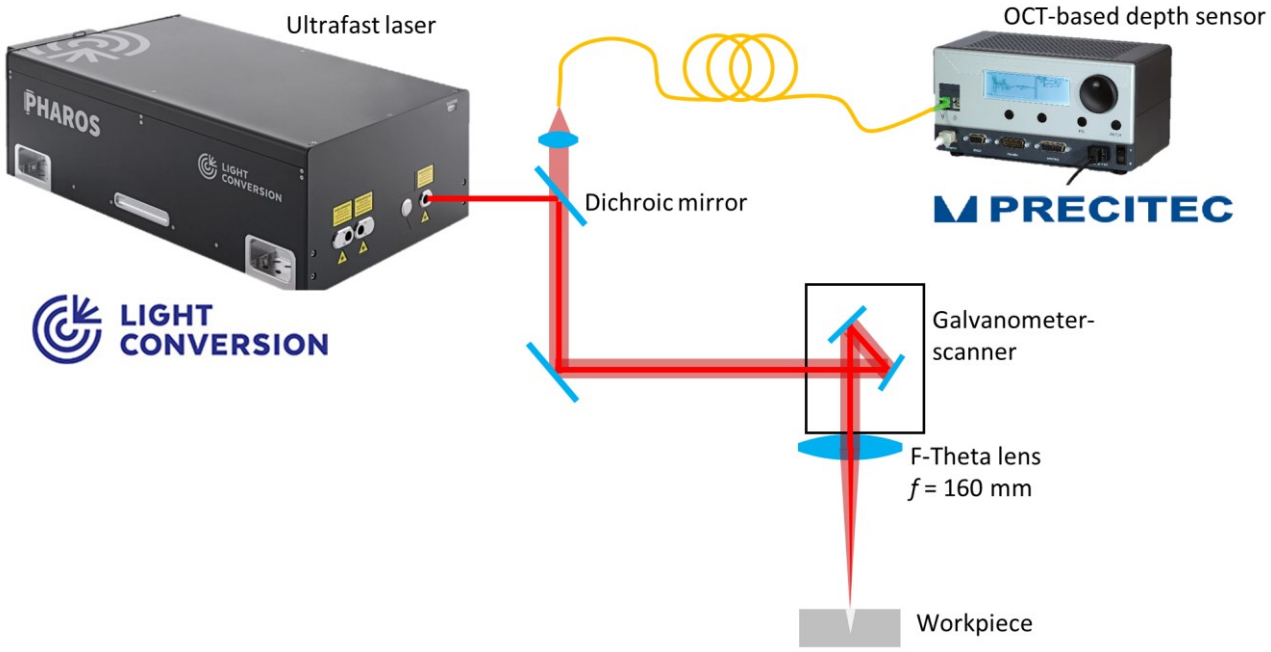

Fig. 1. Experimental setup for online depth-monitoring during laser percussion drilling.

The laser drilling experiments were performed using an ultrafast laser system (Light Conversion, Pharos) with the specifications summarized in Table 1.

Table 1. Specifications of the ultrafast laser.

Parameter	Value
Wavelength	1030 nm
Pulse duration	260 fs
Pulse energy (used in the experiments)	up to 351 µJ
Repetition rate (used in the experiments)	up to 10 kHz
Diameter of beam waist	50 µm

The OCT-based depth sensor enabled in-situ and online depth measurement during drilling. The specifications of the system are summarized in Table 2.

Table 2. Specifications of the OCT-based depth sensor.

Parameter	Value
Wavelength	1080 ±20 nm
Acquisition rate	70 kHz
Axial measurement range	< 6 mm
Axial accuracy	< 30 µm
Diameter of beam waist	15 µm

Advanced signal processing was used on the OCT data, including correction for spatial and temporal offsets, application of a signal-to-noise quality filter, and an "increasing-depth" (ID) filter to ensure reliable depth tracking during high-aspect-ratio hole formation (Holder et al., 2024).

The samples were also characterized by optical microscopy to measure the inlet diameter as well as measure the depth from cross sections. Laser Scanning Microscopy (LSM) enabled detailed topographical imaging of shallow holes, particularly for assessing parabolic geometries and burr heights. Scanning Electron Microscopy (SEM) provided high-resolution imaging of hole morphology, including surface features such as laser-induced periodic surface structures (LIPSS) and melted regions.

3. Results

3.1. Phase 1 - Initiation of the Drilling Process

To evaluate the interaction of ultrashort laser pulses with LPBF-manufactured Ti6Al4V, the ablation threshold ϕ_{th} was determined using the D²-method (or Liu method) based on crater diameters for different number of pulses N_{P}. Fig. 2 shows the measured values for different titanium alloys and similar laser setups.

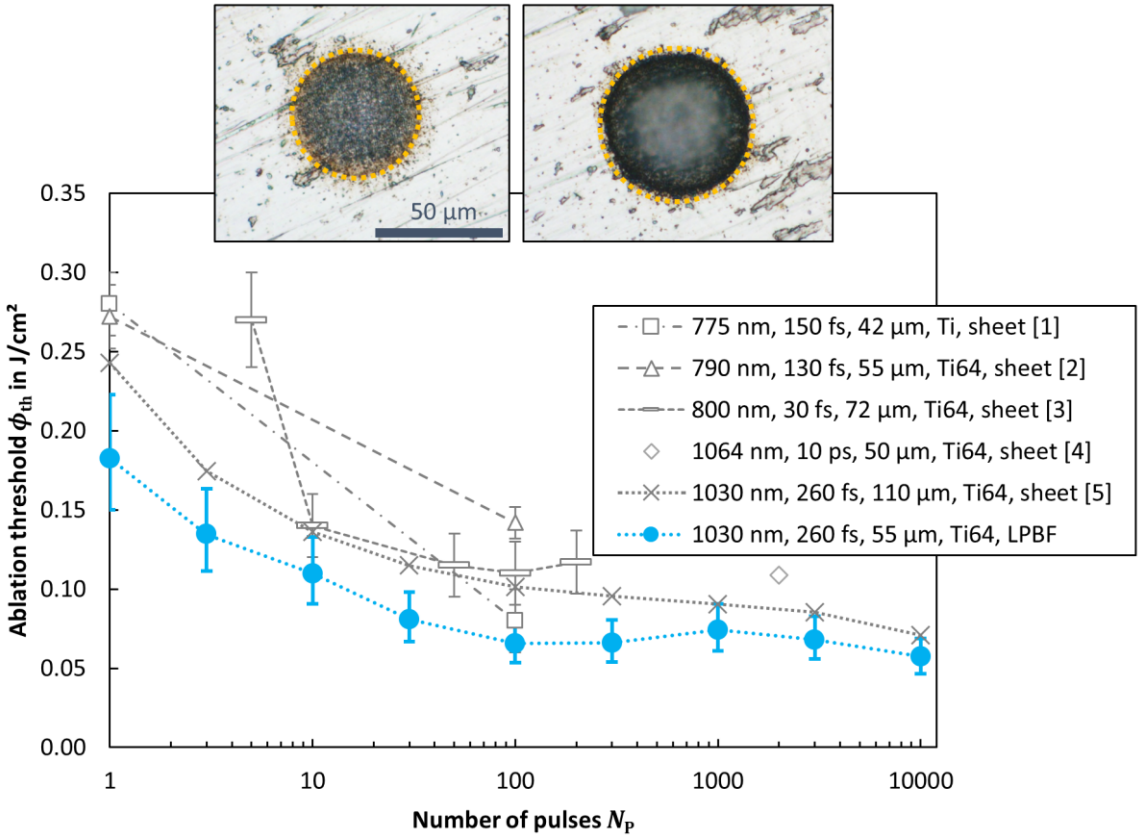

Fig. 2. Ablation threshold measured for different titanium alloys and similar laser setups.

The ablation threshold decreases with increasing number of pulses due to the incubation effect. The comparison with literature data on conventionally produced Ti64 sheets shows that the LPBF-generated sample exhibits a significantly lower ablation threshold. This reduction is presumably attributed to higher surface absorption resulting from increased porosity, microroughness, and possible oxide layers introduced by the LPBF process. Fig. 3 shows the corresponding inlets as measured by SEM. As the number of pulses N_P and the peak fluence ϕ_0 were increased, the morphology of the ablation craters evolved distinctly.

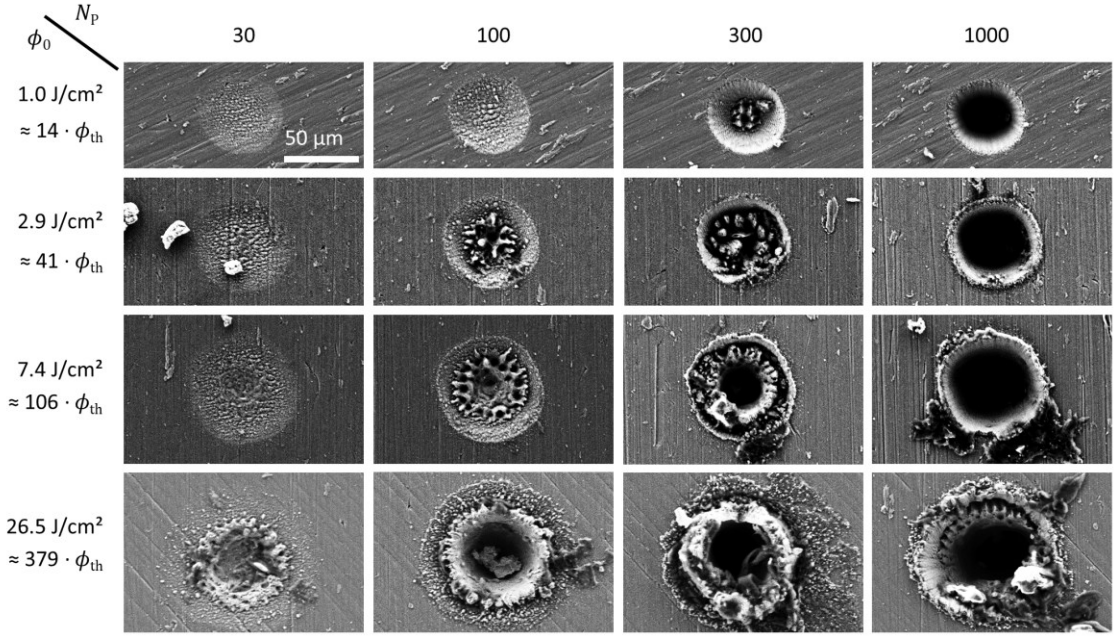

Fig. 3. Inlets measured for different peak fluences ϕ_0 and number of pulses N_P.

At moderate fluence levels (e.g., ~14 · ϕ_{th}), shallow holes with laser-induced periodic surface structures (LIPSS) were observed. Increasing fluence and pulse number led to spike formation, material ejection, and eventually deep holes with burr accumulation at the hole entrance.Fig. 4 shows the maximum burr height as measured by LSM for different combinations of peak fluence and number of pulses.

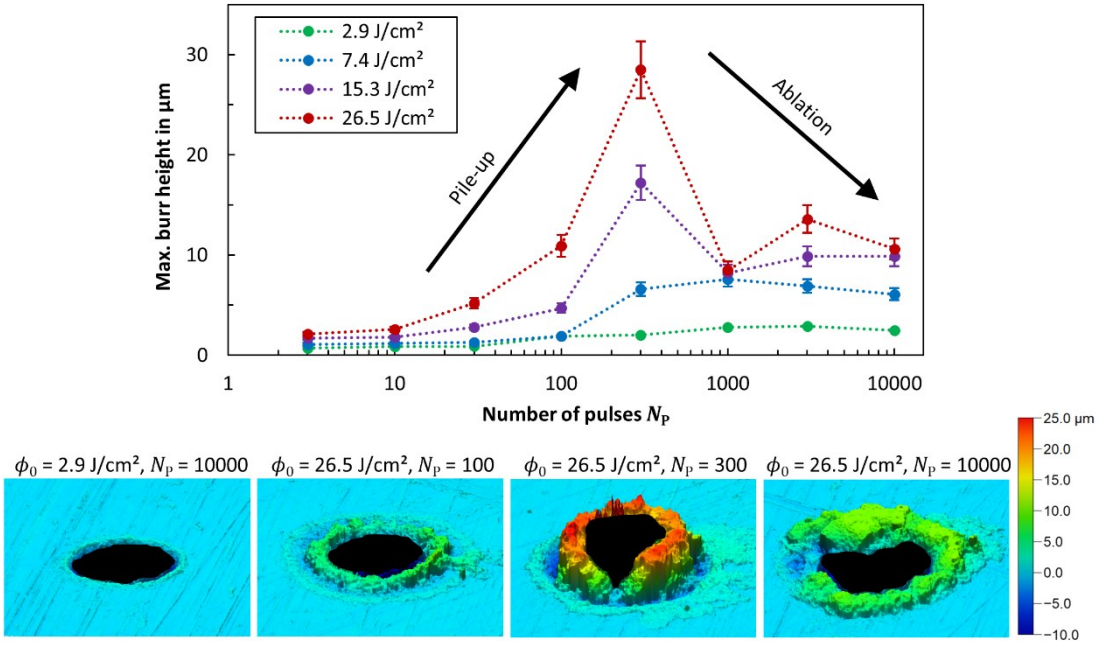

Fig. 4. Max. burr height for different peak fluences and number of pulses.

It can be seen that the maximum burr height increases with increasing number of pulses up to $N_P \approx 1000$ due to pile-up, and decreases thereafter as the piled-up material at the inlet is partially ablated again. Higher peak fluences ϕ_0 lead to a higher pile-up effect.

3.2. Phase 2 - Deep Hole Progression

Fig. 5 shows the hole depth for percussion drilling with up to N_P = 20,000 pulses as measured by optical microscope (from cross sections) and as measured by OCT.

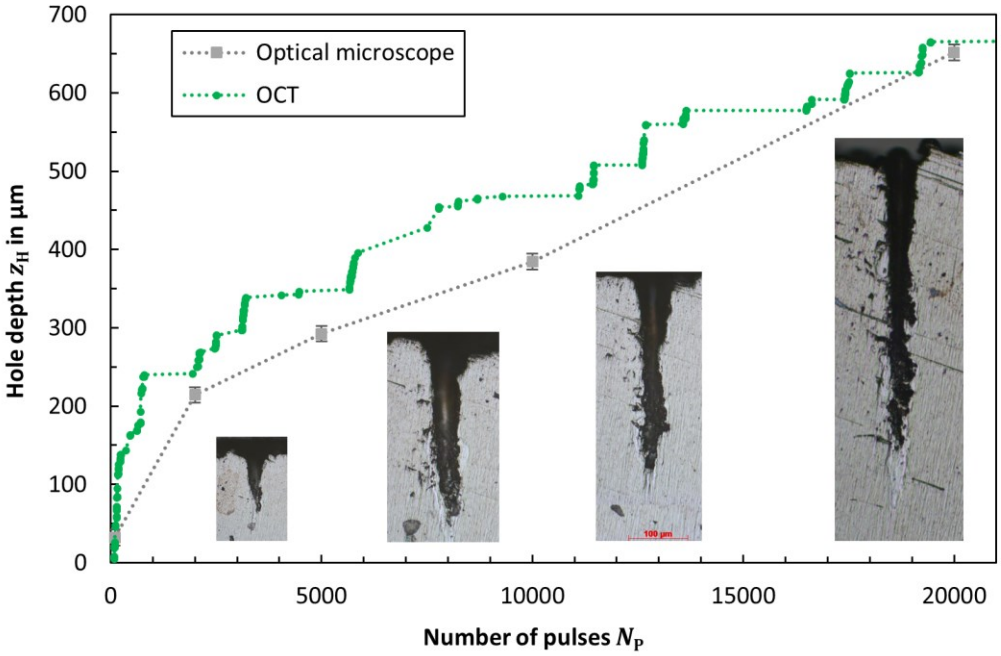

Fig. 5. Evolution of the hole depth for different number of pulses as measured by optical microscope (from cross sections) and as measured by the OCT-based depth sensor.

It is evident that the measurements obtained from the cross sections using the optical microscope frequently result in an underestimation of the hole depth. This is primarily due to the fact that the small tip of the microholes can be readily sanded away during the process of preparing the cross section. OCT-based depth measurements provide real-time depth profiles with high axial and temporal resolution. The measurements reveal intermittent stagnation and nonlinear drilling progression, confirming that physical effects within the hole (e.g., redeposition, plasma confinement) influenced the ablation dynamics.

3.3. Phase 3 - Through-Hole Formation

A series of experiments aimed at producing through-holes in 1.5 mm thick LPBF Ti64 samples revealed the critical dependence on pulse energy. Fig. 6 shows the evolution of the hole depth for deep percussion drilling with up to N_P = 200,000 pulses.

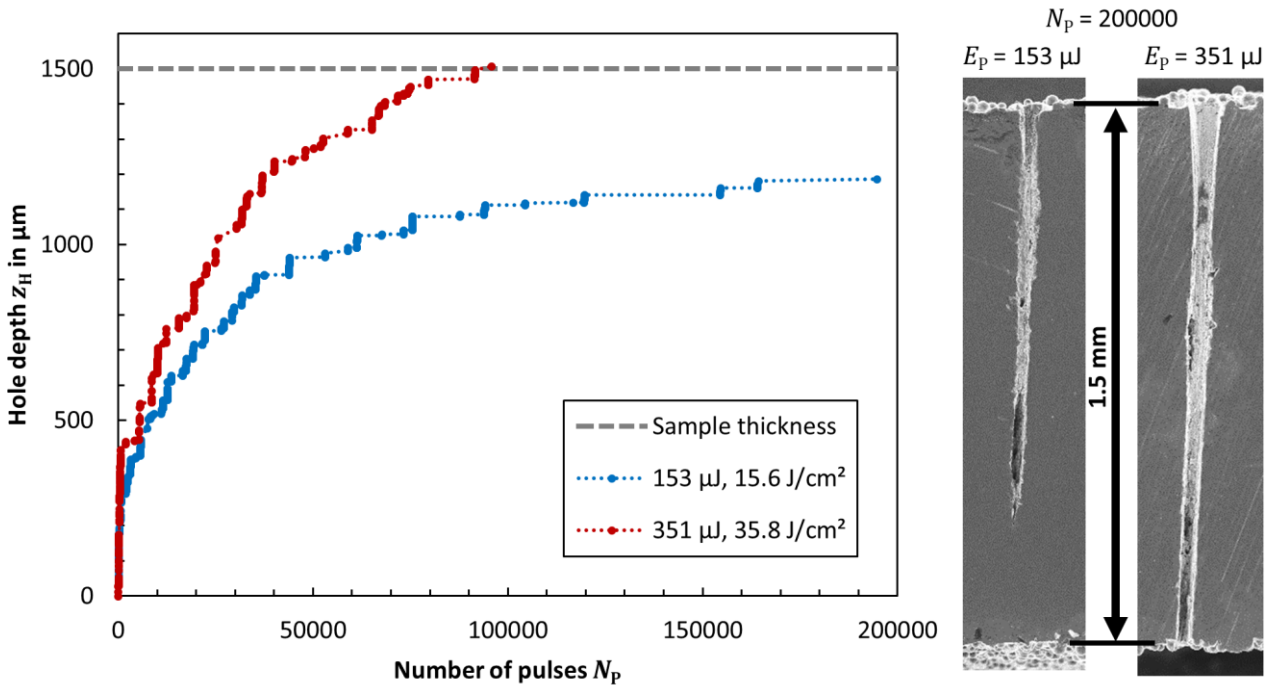

Fig. 6. Evolution of the hole depth for different number of pulses as measured by the OCT-based depth sensor (left) and corresponding hole geometries after N_P = 200,000 pulses (right).

While N_P = 200,000 pulses at E_P = 153 µJ resulted in blind holes, an increased pulse energy of E_P = 351 µJ enabled through-hole formation after approximately N_P = 96,000 pulses.

Fig. 7 (depicted on the next page) shows the corresponding cross section with high magnification insets highlighting three characteristic regions: the top entrance, the middle section, and the exit area. SEM analyses of the through-hole revealed an entrance diameter around 110 µm, narrowing to 55 µm in the central channel, and exit diameters of 40 µm. The overall aspect ratio achieved was approximately 14. The sidewalls show partially ablated powder particles (highlighted with white arrows), and in some cases, axially aligned cracks (highlighted with a black arrow), the origins of which are still under investigation. Contributing factors may include thermal stress, cumulative heat load, and microstructural anisotropy typical of LPBF materials.

4. Conclusion

This work demonstrates the viability and advantages of laser percussion drilling with ultrashort laser pulses for post-processing additively manufactured Ti6Al4V components produced via LPBF. The experimental investigation, structured into three drilling phases - initiation, deep hole progression, and through-hole formation - provides a detailed understanding of the interaction between femtosecond laser pulses and the unique microstructure of LPBF materials.

The key findings include:

- Lower ablation threshold of LPBF Ti64 compared to conventionally produced sheet material, likely due to higher surface absorption from roughness and porosity.
- Emergence of distinct morphological features such as LIPSS, burrs, and spikes during shallow drilling, with burr formation showing a non-monotonic dependence on pulse number.
- Reduced drilling progress in deep hole formation due to plasma shielding, beam attenuation, and ejection limitations.
- Successful integration of OCT-based online monitoring, providing high-resolution depth tracking and revealing localized stagnation phenomena.
- Achievement of through-hole drilling in 1.5 mm thick samples at high pulse energies, reaching aspect ratios up to 14, though accompanied by the formation of axial microcracks.

Overall, ultrashort pulse laser drilling proves to be a powerful subtractive tool to overcome the geometric limitations of LPBF, enabling the production of high-precision microfeatures. Future work will focus on understanding and mitigating defect formation in deep holes, optimizing energy delivery strategies, and integrating feedback control using inline diagnostics like OCT.

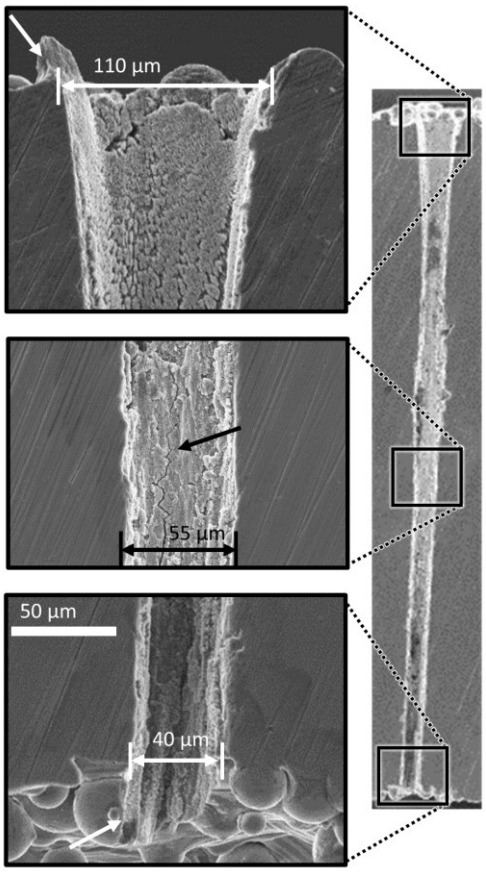

Fig. 7. Microhole percussion drilled with N_P = 200,000 pulses cross-sectioned along its full depth, with high-magnification insets highlighting three characteristic regions: the top entrance, the middle section, and the exit area.

Acknowledgements

The authors would like to thank the German Federal Ministry for Economic Affairs and Energy for funding the research project HolesInOne (03EN4049C) and Precitec for the loan of the OCT-based measurement system CHRocodile 2. The large language model chatGPT 4o from OpenAI was used to improve the language of the text.

References

Holder, D., Klöpfer, R., Hagenlocher, C., Weber, R., Graf, T., 2024. Online determination of the hole depth during drilling with ultrashort laser pulses for depth-adapted drilling strategies, Procedia CIRP 124, p. 649-652.

Holder D., Weber, R., Graf, T., 2021. "Laser micromachining of V-shaped grooves on Ti-6Al-4V with ultrashort laser pulses for passive directional transport of fluids," 40th International Congress on Applications of Lasers & Electro-Optics . Virtual conference, paper #MICRO 103.

Maharjan, N., Zhou, W., Zhou, Y., Guan, Y., 2018. Ablation morphology and ablation threshold of Ti-6Al-4V alloy during femtosecond laser processing, Applied Physics A, 124, 519.

Mannion, P.T., Magee, J., Coyne, E., O'Connor, G.M., Glynn, T.J., 2004. The effect of damage accumulation behaviour on ablation thresholds and damage morphology in ultrafast laser micro-machining of common metals in air, Applied Surface Science 233, p. 275-287.

Xu, S., Chen, Y., Liu, H., Miao, X., Yuan, X., Jiang, X., 2020. Femtosecond laser ablation of Ti alloy and Al alloy, Optik – International Journal for Light and Electron Optics 212, 164628.

Zheng, B., Jiang, G., Wang, W., Wang, K. Mei, X., 2014. Ablation experiment and threshold calculation of titanium alloy irradiated by ultra-fast pulse laser, AIP Advances 4, 031310.